Norwegian
Society of
Chartered Engineers

NORTH SEA FLOW MEASUREMENT WORKSHOP

OCTOBER 22. - 24. 1991
SOLSTRAND FJORD HOTEL, BERGEN - NORWAY

EFFECTS OF FLOW CHARACTERISTICS DOWNSTREAM OF ELBOWS ON ORIFICE METER ACCURACY

Lecturer:

Mr. Kamal Botros
Nova Husky Research Corporation

EFFECTS OF FLOW CHARACTERISTICS DOWNSTREAM OF ELBOW/FLOW CONDITIONER ON ORIFICE METER

U. Karnik, W.M. Jungowski and K.K. Botros
NOVA HUSKY Research Corporation
2928 - 16th Street N.E.
Calgary, Alberta Canada
T2E 7K7

1.0 INTRODUCTION

Flow conditioners are used upstream of orifice meters to eliminate flow non-uniformities and swirl and thereby facilitate accurate metering within a shortest possible meter run. The tube bundle is the most commonly used flow conditioner in natural gas metering. The two important standards providing specifications on the design and locations of the tube bundles are the ANSI/API 2530 and the ISO 5167. An important specification is the straight length section between the piping element generating the disturbance and the flow conditioner (L_1), and that between the flow conditioner and the orifice plate (L_2). These specifications are quite different in the two standards which has led several experimenters and the gas industry to heighten research to study the effects of tube bundle location on orifice meter accuracy.

The available data produced to date, particularly those dealing with elbows generating the flow disturbance upstream, are numerous. Almost all of the published reports and papers attempt to specify a location of the tube bundle between the elbow and orifice meter which gives zero deviation in the orifice discharge coefficient (C_d). The term "cross-over point" is often used to define this optimum location; a shorter distance to the orifice causes a negative ΔC_d while a longer distance causes a positive one.

For this *cross-over* point, contradicting values of L_2/D started to appear (D is the pipe diameter). This was to be expected since the cross-over point is not a unique point for all installations. It should depend on the flow Reynolds number, total length of the meter run, orifice β–ratio, meter tube roughness, and instrumentation among other factors.

To be presented at the 9TH North Sea Flow Measurement Workshop, October 22 - 24, 1991, Bergen Norway

For example, the EC program conducted at Gasunie and NEL for testing the performance of tube bundles in *good flow conditions* has revealed that the cross-over point lies between 10 D and 15 D [1,2]. A similar observation has been made by Brennan, et. al. [3] following experiments performed at NIST (Boulder). Extensive tests by McFaddin, et. al. [4] revealed that, for their meter run, a cross-over point at 17 D was obtained for all β-ratios and was independent of the location of the bundle w.r.t. the disturbance (two elbows in-plane separated by 12 D). Mean velocity profiles at 7 D and 27 D were also presented in [4] which show that although the mean profile at 27 D is nearly fully developed, this was not the optimum position and ΔC_d for the 0.67 and 0.73 orifice plates was around +0.5%. Unfortunately, the velocity profile at 17 D (the cross-over point) was not presented.

Sliding tube bundle experiments were conducted in the low pressure nitrogen loop (724 kPa, $Re = 9 \times 10^5$) of the GRI Meter Research Facility at SwRI [5]. The cross-over point for a 0.75 orifice plate was ≈11 D for 45 D meter run and ≈15 D for 19 D meter run. Velocity profiles measured at different locations revealed that the flow is still far from fully developed in the 45 D meter tube length indicating that there are other factors contributing to the zero shift other than a fully developed velocity profile.

Experiments conducted on the 2" water facility at NIST in Gaithersburg [6] showed that with a tube bundle located at $L_1 = 5.7$ D from elbow outlet, a cross-over point was obtained at ≈12 D for three β-ratios (0.383, 0.5 and 0.75). Measurements of the streamwise and radial mean and turbulent velocity profiles upstream and downstream of the tube, obtained by LDV, showed that the tube bundle produces higher turbulence levels immediately downstream and that the levels reach fully developed (Laufer) values at 27.3 D from tube bundle outlet. Unfortunately, the mean and turbulent velocity profiles were not presented at the 12 D location which could possibly illuminate the contribution of the turbulence levels to the zero deviation of C_d.

In this paper an attempt is made not to produce another cross-over point for an elbow/tube bundle configuration, but to find the underlying mechanistic principles contributing to the optimum location of the tube bundle w.r.t. the orifice meter. Tests were conducted on NOVA's high pressure test facility at Didsbury, Alberta, Canada. The flow Reynolds number based on pipe diameter was $\approx 8 \times 10^6$. Two elbows in-plane separated by 10 D represented the disturbing element, and a 2.5 D long tube bundle (19 tubes) sliding along the pipe was used in the experiments. Mean velocity profiles were obtained by means of a Pitot-static tube traversing in two planes. Tests on a similar configuration were conducted in a low pressure air loop where profiles of the mean velocity and the Reynolds stresses were obtained by hot-wire anemometry.

In this paper, results from both the high pressure and low pressure facilities are presented and a preliminary conjecture on the effects of turbulence and shear stress distribution downstream of a tube bundle on the C_d shifts is proposed. An attempt is made to correlate the contribution of the mean velocity profile, turbulence level, and shear stress to the location of the cross-over point.

2.0 EXPERIMENTAL FACILITIES

High Pressure Facility

A schematic of NOVA's Gas Dynamic Test Facility at Didsbury, Alberta, Canada is shown in Figure 1. High pressure natural gas is diverted from the mainline into the test loop by means of a centrifugal compressor or in a free flow mode. The maximum operating pressure at the facility is 6450 kPa and the maximum Reynolds number in the test section of a 100 mm diameter was $\approx 8 \times 10^8$. The test section is shown in more detail in Figure 2. Two orifice fittings are installed in series, the one upstream being the reference meter. This reference orifice meter is preceded by 44 D straight meter run of internal roughness $\approx$5.0 µm Ra, and two reducers 200 x 150 mm and 150 x 100 mm with 16 D separation. Two elbows in-plane with 10 D separation are shown in Figure 2. Both in-line tube bundle or a sliding tube bundle were used upstream of the second (tested) orifice meter. The second orifice fitting is replaced with a traversing mechanism holding a standard Pitot-static tube (PST) when measuring the axial and transverse velocity profiles. High-accuracy transmitters were used in measuring the differential pressures across the flange-tapped orifices and also the static pressure to an accuracy of ±0.1% of span. As for the PST, the differential pressure transmitter connected to the stagnation and static holes is calibrated in the range of 1 to 12.5 kPa, while the static holes (for radial velocity component) differential transmitter was calibrated between - 1.5 to + 1.5 kPa. All velocity profiles were normalized by the instantaneous mean flow velocity obtained by the reference orifice meter upstream. Temperature accuracy is within ±0.2% of the span. A gas chromatograph is connected on line to give detailed gas composition of the gas during the course of the experiments.

Low Pressure Facility

The low pressure test facility consists of a 100 mm diameter test section, calibrated sonic nozzle and 30 kW blower. Air is driven through the test section in a suction mode as shown in Figure 3a. Experiments were conducted with a sonic nozzle securing mean velocity of approximately 14.7 m/s through the test section, resulting in a Reynolds number of $\approx 0.9 \times 10^5$. Mean and turbulent velocity profiles as well as shear stresses were obtained by x-wire miniature probe with

a TSI anemometer (IFA 100). The x-wire was calibrated in a TSI calibrator. Figure 3a shows the test section for a fully developed turbulent flow measurements at ≈68 D downstream of a sprenkle plate following the inlet filter. This test section was used to evaluate the performance of the 19 tube flow conditioner in a good flow condition. Figure 3b shows the test section altered with an upstream elbow of radius 1.5 D and an in-line tube bundle. The x-wire was traversed across two perpendicular planes at 19 D from elbow outlet, for different location of the tube bundle. Figure 3c shows similar configuration with a sliding tube bundle and an orifice meter located at 19 D from the elbow outlet. The reference flow is measured by the calibrated sonic nozzle downstream. All pipes used in the low pressure experiments were clear PVC pipes with internal roughness around 0.25 μm (Ra). The elbow, however, is exactly the same steel elbow used in the high pressure facility.

3.0 RESULTS FROM HIGH PRESSURE FACILITY

At the high pressure test facility the Pitot-static tube was traversed in a vertical and horizontal plane. The measurements were taken at various distances from the second elbow: a) without any flow conditioner, b) 4 D downstream of the tube bundle outlet with the tube bundle at different positions from elbow outlet, c) with fixed position of the tube bundle inlet at 2 D from the elbow and PST at different locations downstream, and d) with fixed position of the PST at 19 D from the elbow and moved tube bundle.

The following observations were made:

re: a) the profiles acquired close to the second elbow outlet were typical for a single elbow configuration, they became flat at about 16 D and then more elongated at 27.6 D but still deviating from the reference profile which was measured upstream of the elbows in the straight pipe (Figure 4);

re: b) velocity profiles varied significantly with increasing distance between the elbow and tube bundle outlets until around 12.5 D and then the pattern was primarily determined by the distortion by the tube bundle itself (Figure 5);

re: c) the profiles at 6 D from the tube bundle outlet revealed strong distortions and at 27.6 D became rather uniform but more elongated than the reference profile (Figure 6);

re: d) with decrease in distance from 15 to 5 D between the elbow and tube bundle outlets, the profiles changed from an underdeveloped character to a more elongated one (Figure 7).

In order to correlate the velocity profiles to the cross-over point, the PST was replaced by an orifice plate and the flow rate was metered with various positions of the tube bundle as in case d). As Figure 8 shows, the cross-over occurred around L_2 = 8D for both orifice plates (β = 0.4 and 0.74). However, the corresponding vertical and horizontal profiles were underdeveloped compared to the reference profile. In order to characterize the reference profile, the distribution of the wall static pressure along the upstream pipe of the reference meter was measured. The reference profile was found previously when the reference meter was substituted with the pitot tube. Figure 9 shows a quasi-linear pressure drop along the pipe indicating that the flow is fully developed. Utilizing Darcy friction factor f = 0.0131 evaluated from the pressure drop and the approximate relation $n = 1/\sqrt{f}$ [14] between the exponent n characterizing the velocity profile and f, n = 8.74 was found. This relation, however, overestimates n by about 10%. On the other hand, the fit to the experimental reference profile (Figures 4 through 7) gave n = 7.83. Both results appear to agree well.

A few conclusions can be drawn from the study performed at the high pressure facility. A comparison of case a) with c) indicated that an enhancement of turbulence by the tube bundle significantly increased the rate of the velocity profile modification, even to the overdevelopment. Case b) showed that at a certain distance, distortion caused by the tube bundle dominates the effect caused by the elbows. This confirms earlier observations in [2,3,4] that the upstream distance L_1 has less effect than L_2 on metering error. However, placing the tube bundle close to the elbow outlet tends to freeze the incoming velocity profile and defeat the purpose of the tube bundle. Case d) and metering with the orifice plate revealed that the cross-over point can occur with different mean velocity profiles. This implies that some other factors contribute to the outcome of flow metering. The analysis of momentum equations pointed to the distribution of the Reynolds stresses and therefore gave an incentive to measure turbulence. Preparation for these measurements at the high pressure facility is currently underway.

In the meantime, in order to simplify experimental procedures and understand the flow characteristics, tests were conducted on the low pressure test facility. It is believed that these results could be scaled to the high pressure/high Re flows.

4.0 RESULTS FROM LOW PRESSURE FACILITY

4.1 Reference Profiles

Reference profiles were obtained, following a development length of approximately 68D, with the use of a miniature x-wire probe (see Figure 3a). The average velocity for this flow was around 14.7m/s resulting in a Reynolds number of $\approx 0.9 \times 10^5$. It can be seen from Figure 10 that the mean axial velocity profiles are nearly axi-symmetric and that the measurements are compatible with the power law

$$\frac{U}{U_{max}} = \left(\frac{y}{R}\right)^{1/n}.$$

A log-log plot of (y/R v/s U/Umax) revealed that the value of n in the above power law is ≈ 7.4. Measurements close to the wall and near the centerline were excluded for the regression. The "expected" value of n for a smooth pipe at $Re=0.9 \times 10^5$ is around 7.0. Thus, the present profile may be regarded to be slightly under-developed.

It has been shown, analytically [7] and experimentally [8,9], that for a fully developed flow the distribution of the turbulent shear stress (τ_t) across the pipe diameter is linear and its extrapolation to the wall would result in an estimation of the wall shear stress. Figure 11 shows our measurements of the turbulent shear stress $\overline{uv} = \tau_t/\rho$. The distribution is clearly linear. This indicates that, for all practical purposes, the flow is fully developed. The shear stress is zero at the center as expected and on extrapolating this distribution to the wall, the wall shear stress (τ_w/ρ) is estimated to be approximately $0.42 m^2/s^2$ resulting in a friction velocity (u_*) of 0.65m/s. Thus, if the measured wall shear stress is used to normalize the data, the shear stress distribution (Figure 12) is representative of a fully developed flow. Additionally, the distribution of the correlation coefficient ($\overline{uv}/u'v'$) is akin to that observed in a fully developed flow [8,9] where u' and v' are the rms values of the fluctuating axial and radial velocities. The correlation coefficient reaches an asymptotic value of approximately 0.43 near the wall. This value was measured as 0.4 and 0.5 by [9] and [8] respectively. The correlation coefficient is usually approximated to be around 0.45 for a boundary layer [10].

The axial and radial rms turbulent intensities, presented in Figure 13 are found to be comparable to Laufer's data [8]. The axial intensities appear to be slightly higher, however, a similar observation was made by Lawn [9], who measured intensities higher than those measured by Laufer [8] and those measured in the present experiments.

Thus, measurements at the reference location appear to indicate that, for all practical purposes the present flow is fully developed. Apart from providing details of the reference velocity field, these measurements have also served as a test of credibility for the data acquisition and post processing of the hot-wire anemometer signals.

4.2 Measurements Downstream of a Tube Bundle in Good Flow Conditions

Measurements downstream of a 19 tube tube bundle (circular pattern, d_i=18 mm, d_0=20 mm, 2.5D long) were obtained with the above reference profile as an input.

The mean axial velocity profiles at various locations downstream of the tube bundle are shown in Figure 14, normalized by the maximum measured velocity. Allowing for experimental inaccuracies, these profiles indicate that, after the initial decay of the jets/wakes generated by the tube bundle, the velocity profiles are nearly compatible with the reference profile (n=7.4) after 6 pipe diameters.

Profiles of the axial and radial rms turbulent velocities (normalized by the maximum velocity), at locations downstream of the tube bundle, are shown in Figures 15a and 15b, respectively. As expected, the turbulence intensities are maximum at the location closest to the tube bundle. These intensities decay at downstream locations to a level below that at the reference location and exhibit a growth further downstream. A similar behavior, on the centerline, has been observed by Morrow et. al. [17] in their sliding vane measurements. In their case, the tube bundle was placed downstream of a single elbow. The variation of the normal stresses on the centerline with downstream location, shown in Figure 16, indicates that the position of the minima is at 10 D from tube bundle outlet

This behavior of initial decay and subsequent growth of the normal stresses is consistent with the physics of the flow. Initially, the tube bundle generates high normal stresses (turbulence) due to the shear of the jets/wakes generated. As these jets/wakes coalesce, turbulence decays according to a power law in a manner similar to grid turbulence (Sreenivasan et al. [11], and Warhaft, [12]). This decay dominates the production of the pipe boundary layers until a balance is reached. Subsequently, turbulence grows and, in the case of a pipe flow, it should be expected to reach the fully developed magnitude asymptotically. This behavior of initial decay and subsequent growth in the presence of a uniform shear, has also been documented in the wind tunnel

experiments of Tavoularis and Karnik [13]. However, in their case, due to the presence of a uniform shear, turbulence continues to grow downstream.

It may be worthwhile to note that the initial rate of decay of grid turbulence is dependent on the mesh size ($M = d_i$ in our case) of the grid and on the initial Reynolds number ($Re_M=UM/\upsilon$). Since decay of energy is mainly attributed to the draining of energy from the large eddies towards the smaller eddies via inertial interactions [14], a smaller mesh size would imply a quicker decay of energy. Also, in terms of the initial Reynolds number, a higher Reynolds number implies lower viscous dissipation due to either lower kinematic viscosity or a slower energy transfer due to larger scales (larger mesh size). This is evident from the measurements of Batchelor and Townsend [15] (Re_M upto 4.4×10^4) and those of Kistler and Vrebalovich [16]($Re_M=2.4\times10^6$).

Measurements of the turbulent shear stress (Figure 17) reveal that the linear distribution of the incoming reference flow has been distorted. Initially, the shear stress changes sign, as expected, at locations of the jets/wakes. The shear stress is high at the locations of the maximum velocity gradients and the change of sign is at the location where the mean velocity gradient is zero. Further downstream, the shear stress begins to re-organize itself. The magnitude of the shear stress is low in the core of the flow due to a lower mean velocity gradient and increases towards the pipe walls. Further downstream, at about x/D=13, the shear stress appears to be re-aligning itself with the reference shear stress distribution (shown as solid line). Hence it is evident that although the mean velocity profile appears to be fully developed, the non-linear shear distribution indicates otherwise.

4.3 Measurements Downstream of a Tube Bundle with a Single 90^0 Elbow

As mentioned earlier, these measurements were conducted to simulate the high pressure facility and understand the contribution of turbulence to metering error. The major differences in the two facilities are the working pressure, test fluid and the pipe Reynolds number. The present measurements were taken downstream of a tube bundle, described earlier, with the velocity profile from a single 90^0 elbow (r=1.5D) as in input.

Mean axial velocity profiles for the three different locations of the tube bundle with respect to the elbow in a 19D meter run are shown in Figure 18. The velocity profile at the location of the orifice plate appears to be dependent on the distance of the tube bundle from the elbow. For locations closest to the elbow (L_2=10 D), the reminence of the effect of the elbow is evident

whereas at the location farthest from the elbow (L_2=4 D), the velocity profile downstream of the tube bundle is relatively flat indicating that the effects of the elbow are sufficiently diminished.

The above can also be concluded from the velocity profiles obtained at the high pressure facility. However, it appears that comparison of the velocity profiles in the two situations may not be possible due to differences in the Reynolds number. As mentioned earlier, the dissipation due to viscous action is less at higher Reynolds numbers and hence one could speculate that the effects of the elbow and tube bundle would diminish at downstream distances which are longer than those in the case of lower Reynolds numbers. This can be seen from the fact that at the high pressure facility (high Re), for L_2=4 D, the wakes/jets of the tube bundle are clearly detected (Figures 6 and 7), however, in the case of the low pressure facility for a similar configuration, there is no evidence of the presence of these wakes/jets.

As observed in the case of the tube bundle in good flow conditions and by Morrow et. al. [17], the axial and radial turbulence intensities in the present case are found to be lower than the reference values as seen in Figures 19 and 20. The shear stress (Figure 21) also exhibits a non-linear distribution similar to that seen in the case of a tube bundle in good flow conditions. It is worth mentioning at this point that the gradient of the shear stress away from the centerline appears to be greater than that for the reference flow.

In order to determine the cross over points of the C_d shift, the tube bundle pulling mechanism used in the high pressure facility was utilized for the present measurements. The orifice plate (β=0.44) was located at 19D from the elbow and the flow was metered by means of a calibrated sonic nozzle. In order to obtain a pressure drop across the orifice plate within the range recommended (10 to 40 kPa) the chosen sonic nozzle resulted in a Reynolds number of $\approx 1.4 \times 10^5$. The pressure taps for the orifice plate were located in the horizontal and vertical plane at r/R = -1.0. For each location of the tube bundle the % error in the flow rate and C_d was evaluated

Results of the comparative testing, shown in Figure 22., indicate that there exists a cross-over point at approximately 1.5D and another at around 6D. Also, the vertical pressure taps (in the plane of the elbow) consistently appear to read a lower pressure differential than the horizontal pressure taps indicating that the plane of location of the pressure taps is important when considering orifice metering accuracy.

5.0 ANALYSIS OF RESULTS

The first cross-over point at x/D=1.5 of Figure 22 is not surprising. At positions closer than 1.5D, the pressure has not fully recovered from the pressure drop due to the tube bundle, hence, the upstream pressure tap is subjected to lower pressure levels resulting in a positive shift in the discharge coefficient. As the tube bundle is retracted, at around 1.5D, pressure recovery takes place and levels of pressure are akin to the true pressure levels and a zero error (first cross over) occurs.

With further pulling of the tube bundle, the pressure has fully recovered from the tube bundle effects, and other parameters must be sought to explain the non-zero errors in the discharge coefficient. Previously, only the mean axial velocity profile has been used to explain this occurrence. It has been claimed that if the mean velocity profile is close to being fully developed, then a zero error would occur. However, deviations from this claim have been noticed. For example, measurements at the high pressure facility show that the mean horizontal velocity profile at the cross-over point is rather flat. We mention the horizontal profiles since the taps are on the horizontal plane. On the other hand, the profiles presented at 27D downstream of the tube bundle by NIST [4] indicate that the mean velocity profile is nearly fully developed and yet an error of +0.5% occurs in the discharge coefficient. Such contradictions have been stimulous to measure and document the turbulent stresses in the present work and if possible extend the correlation of the metering error to the turbulent structure of the flow.

Although more *"carefully planned and controlled"* experiments would be required to establish an exact relation between metering error and the turbulent structure, at this stage it suffices to show that there exists such a relationship and we propose what may possibly be viewed as conjectures based on the limited information in hand in the following.

Consider the mean axial momentum equation which can be written as [14]

$$\rho\frac{DU}{Dt} = -\frac{\partial P}{\partial x} + \mu\nabla^2 U - \rho\frac{\partial \overline{u^2}}{\partial x} - \frac{\rho}{r}\frac{\partial r\overline{uv}}{\partial r} - \frac{\rho}{r}\frac{\partial \overline{uw}}{\partial \theta} + F_x$$

where U,V and W are the mean velocities in the axial, radial and azimuthal directions and u,v and w are the corresponding fluctuating velocities.

For a steady, axisymmetric flow with negligible body forces the above equation can be simplified to

$$\frac{1}{2}\frac{\partial\left(\rho U^2\right)}{\partial x} = -\frac{\partial P}{\partial x} + \mu\frac{\partial}{\partial r}\left(\frac{\partial U}{\partial r}\right) + \frac{\mu}{r}\frac{\partial U}{\partial r} + \mu\frac{\partial}{\partial x}\left(\frac{\partial U}{\partial x}\right) - \rho\frac{\partial\overline{u^2}}{\partial x} - \frac{\rho}{r}\frac{\partial r\overline{uv}}{\partial r}$$

The above equation can then be re-written as

$$\frac{\partial P}{\partial x} = \left(\frac{\partial \tau_L}{\partial r} + \frac{\tau_L}{r}\right) + \left(\frac{\partial(-\rho\overline{uv})}{\partial r} + \frac{-\rho\overline{uv}}{r}\right) + \mu\frac{\partial}{\partial x}\left(\frac{\partial U}{\partial x}\right) - \frac{\partial\rho\overline{u^2}}{\partial x} - \frac{1}{2}\frac{\partial\left(\rho U^2\right)}{\partial x}$$

where the laminar shear stress is given by

$$\tau_L = \mu\frac{\partial U}{\partial r}$$

the quantity $-\rho\overline{uv}$ is the turbulent shear stress and $\overline{u^2}$ is the axial normal stress.

It is evident that the pressure field is not only coupled to the mean velocity, but also to the Reynolds stresses. Consider the following conjectures, based on the above equation, to explain the effects of the mean and turbulent velocities on the pressure difference across the orifice.

Having already explained the reasons for the first cross over point at 1.5D, consider the following explanation for the second cross-over point at 6D. Consider the profiles for the case (L_2 = 4 D), which is close to the second cross-over point. An examination of the above momentum equation as applied to the flow upstream of the orifice plate reveals that when the mean velocity profile approaching the orifice is flatter than the fully developed, the magnitude of the pressure gradient will be lower resulting in higher pressure levels at the upstream tap (hence higher Δp across the orifice). The same applies to the contribution of the turbulence level $\overline{u^2}$; lower values upstream of the orifice tend to increase Δp. On the other hand, if one extrapolates the shear stress measurements to the wall (Figure 21), then the resulting wall shear stress appears to be higher than the fully developed value. Also, the gradient of the shear stress is shown to be higher at the wall compared to that for a fully developed flow (Figure 21). Therefore, both a higher level of the shear stress and higher gradient at the wall would result in reducing Δp. This counteracting behavior could result in a cancellation effect resulting in a pressure level that produces a cross-over point.

For the intermediate location (L_2=8 D), the mean velocity profile approaching the orifice plate appears to be nearly fully developed. Once again, in applying the momentum equation the mean velocity inertial terms can be neglected. The decay of the normal Reynolds stresses tend to increase the pressure levels at the upstream tap, however, the gradient of the shear stress which is considerably greater than its fully developed counter part tends to reduce this pressure. The latter effects is more severe, resulting in a low differential pressure across the orifice plate and consequently a positive shift in the discharge coefficient.

In conclusion, as stated before, in the absence of more in-depth measurements, the above explanations may be viewed as conjectures, at best, however, they seem to adequately explain metering error which thus far could not be done solely on the basis of the mean velocity field. Finally, the present measurements and their interpretations most certainly illuminate the fact that there exists a definite relationship between orifice metering error and the turbulent velocity field.

6.0 FUTURE WORK

It is evident that there exists a need to conduct carefully planned and in-depth measurements to shed more light on the precise interaction between orifice metering errors and the mean and turbulent velocity field. Apart from the Reynolds stresses, also of interest are the measurements of the integral length scales and the Taylor (dissipation) microscale. These would provide information on the effect of initial scale size (due to tube bundle) on the decay of energy. Such experiments are being planned at the low pressure facility at NHRC. Also, this study is to be extended to the high pressure facility. Although equipment problems have been taken care of with regards to the functioning of the IFA 100 in natural gas application at high pressures, approval is currently being sought from the appropriate agencies to use this technique at such a hazardous location. Once this has been achieved, it will then be possible to document the mean and turbulent velocity flow field for low and high Reynolds numbers. This should go a long way towards shedding light on the interaction of orifice metering error and the velocity field.

7.0 ACKNOWLEDGEMENT

The authors would like to acknowledge the assistance provided by P.Goldsmith, S.Fry and P.Tetreau during the experiments. The work presented here is part of a flow metering research program sponsored by NOVA CORPORATION OF ALBERTA and the permission to publish it is hereby acknowledged.

8.0 REFERENCES

1. Smith, D.J.M., "The Effects of Flow Straighteners on Orifice Plates in Good Flow Conditions", Commission of the European Communities, Directorate - General, Telecommunications, Information Industries and Innovation, Batiment Jean Monnet, Luxembourg, 1986.

2. Sattary, J.A., "EEC Orifice Plate Programme - Installation Effects", Seminar on Installation Effects on Flow Metering, NEL, Glasgow, 1990.

3. Brennan, J.A., Sindt, C.F., Lewis, M.A. and Scott, J.L., "Choosing Flow Conditioners and their Location for Orifice Flow Measurement", Seminar on Installation Effects on flow Metering, NEL, Glasgow, 1990.

4. McFaddin, S.E., Sindt, S.F., and Brennan, J.A., "Optimum Location of Flow Conditioners in a 4" Orifice Meter", National Institute of Standards and Technology, Chemical Engineering Science Division, Boulder, Colorado, 1989.

5. Morrow, T.B., "Determination of Installation Effects from 100 mm Orifice Meter Using a Sliding Vane Technique", Seminar on Installation Effects on Flow Metering, NEL, Glasgow, 1990.

6. Mattingly, G.E., and Yeh, T.T., "Effects of Pipe Elbows and Tube Bundles on 50 mm Orifice Meters", Seminar on Installation Effects on Flow Metering, NEL, Glasgow, 1990.

7. Tennekes, H., and Lumley, J.L., "A First Course in Turbulence", MIT Press, 1972.

8. Laufer, J., "The Structure of Turbulence in Fully Developed Pipe Flow", NACA Report 1174, 1954.

9. Lawn, C.J., "The Determination of the Rate of Dissipation in Turbulent Pipe Flow", J. of Fluid Mechanics, Vol. 8, Part 3, 477-505, 1971.

10. Schlichting, H., "Boundary-Layer Theory", McGraw-Hill, New York, 1979.

11. Sreenivasan, K.R., Tavoularis, S., Henry, R., and Corrsin, S., "Temperature Fluctuations and Scales in Grid-Generated Turbulence", J. Fluid Mechanics, Vol. 100, Part 3, 597-621, 1980.

12. Warhaft, Z., "The Interference of Thermal Fields from Line Sources in Grid Turbulence", J. Fluid Mechanics, Vol. 144, 363-387, 1984.

13. Tavoularis, S. and Karnik, U., "Further Experiments on the Evolution of Turbulent Stress and Scales in Uniformly Sheared Turbulence", J. Fluid Mechanics, Vol. 204, 457-478,1989.

14. Hinze, J.O. "Turbulence", 2nd Edition, McGraw Hill, New York, 1975.

15. Batchelor, G.K. and Townsend, A.A., "Decay of Isotropic Turbulence in the Initial Period", Proc. Roy. Soc. London, 193A, 539, 1948.

16. Kistler, A.L. and Vrebalovich, T., J. Fluid Mechanics, Vol. 26, 37, 1966.

17. Morrow, T.B., Park, J.T., and McKee, R.J., "Determination of Installation Effects for a 100 mm Orifice Meter Using a Sliding Vane Technique". Flow Meas. and Inst., Vol. 2, No. 1, Jan. 1991.

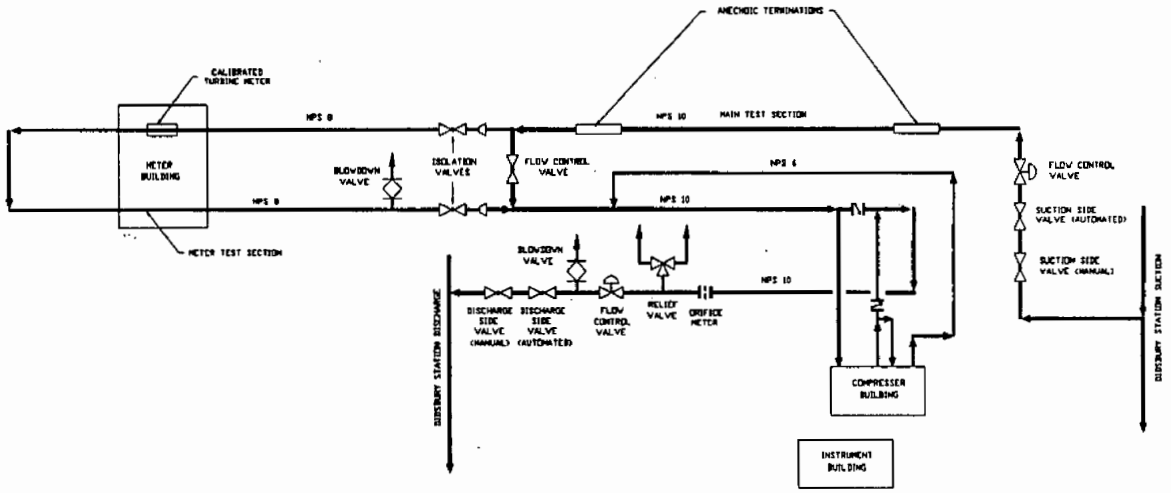

Fig. 1: NOVA's High Pressure Test Facility at Didsbury, Alberta, Canada

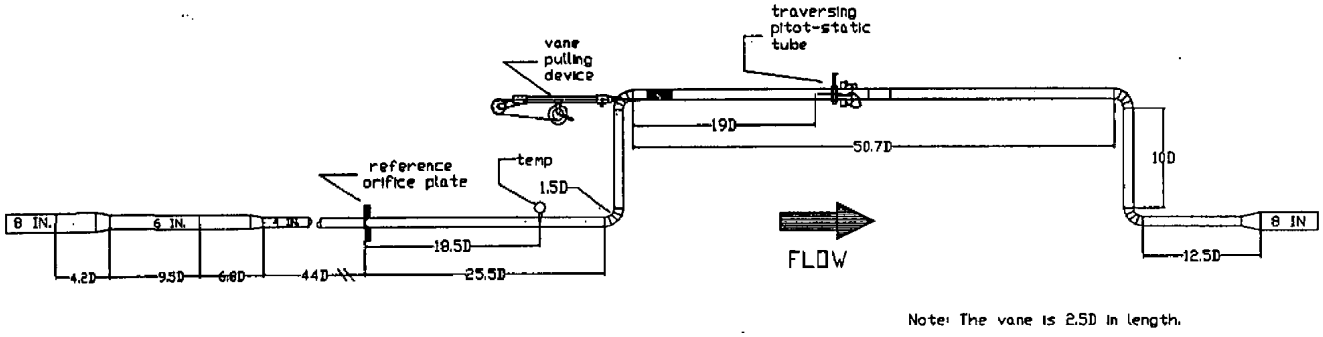

Fig. 2: Test Section Arrangement in the Meter Room of Fig. 1

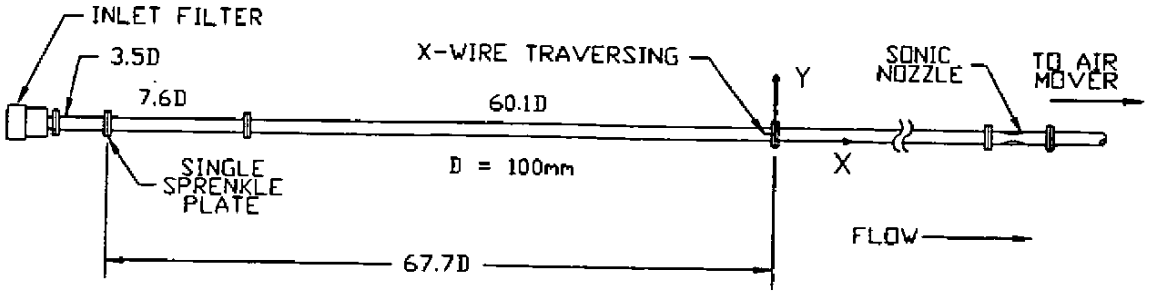

Fig. 3a: Low Pressure Test Facility - Good Flow Conditions

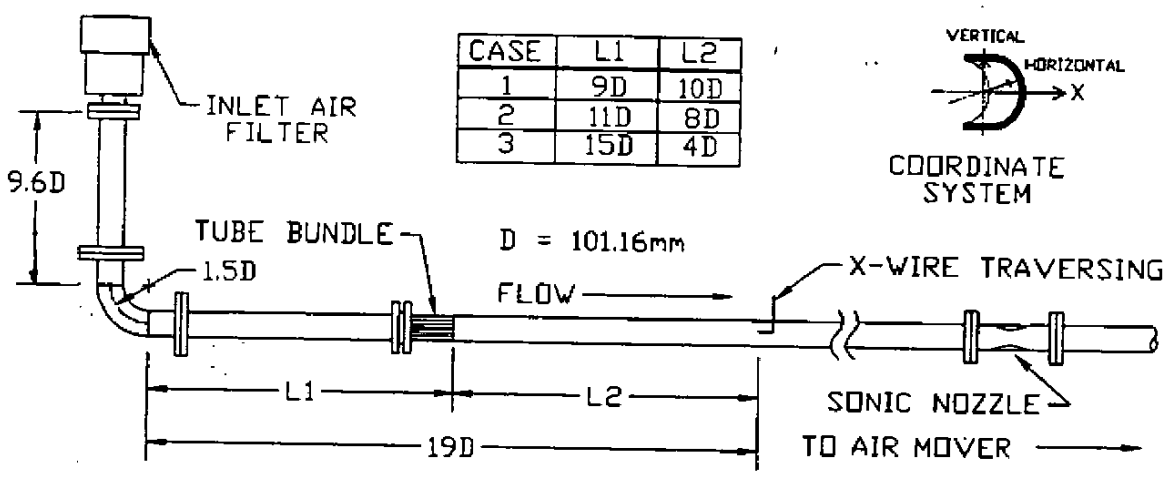

Fig. 3b: Low Pressure Test Facility - Elbow and In-line Tube Bundle

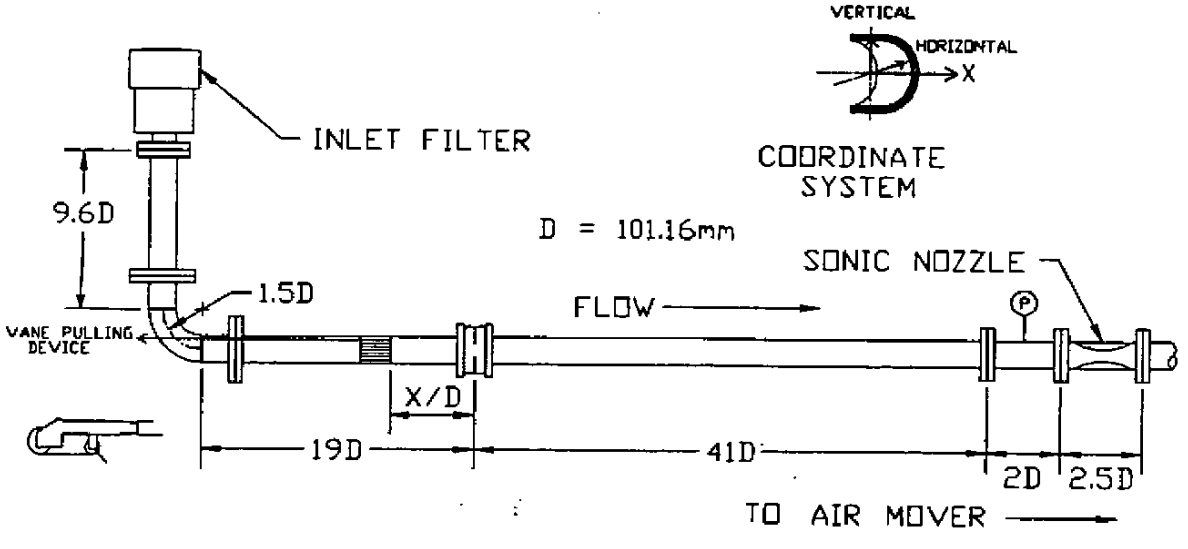

Fig. 3c: Low Pressure Test Facility - Elbow and Sliding Tube Bundle

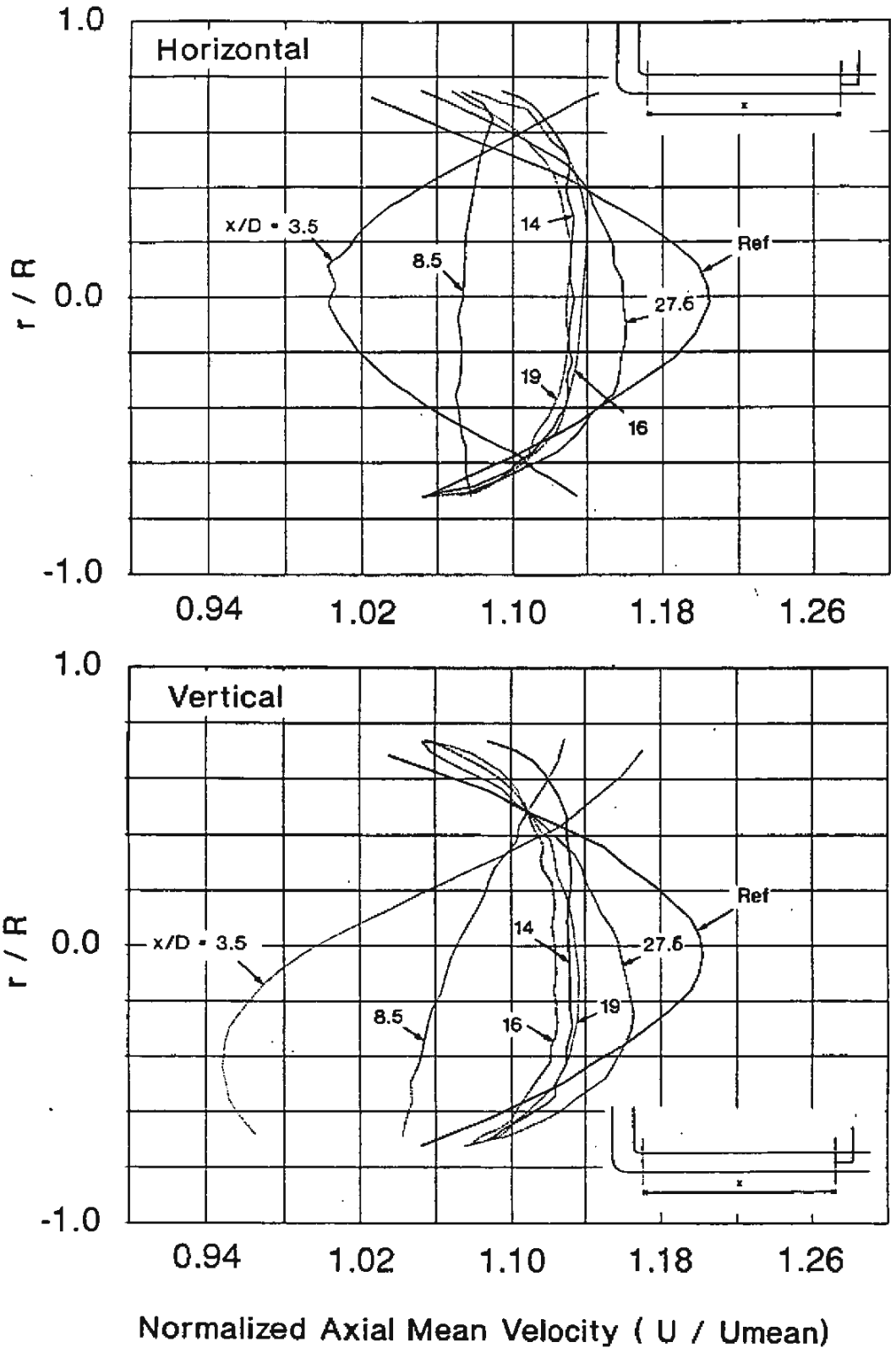

Fig. 4: **Axial Velocity Profiles in the Horizontal and Vertical Planes Downstream of Two Elbows In-plane Without Flow Conditioner ($Re = 8 \times 10^6$)**

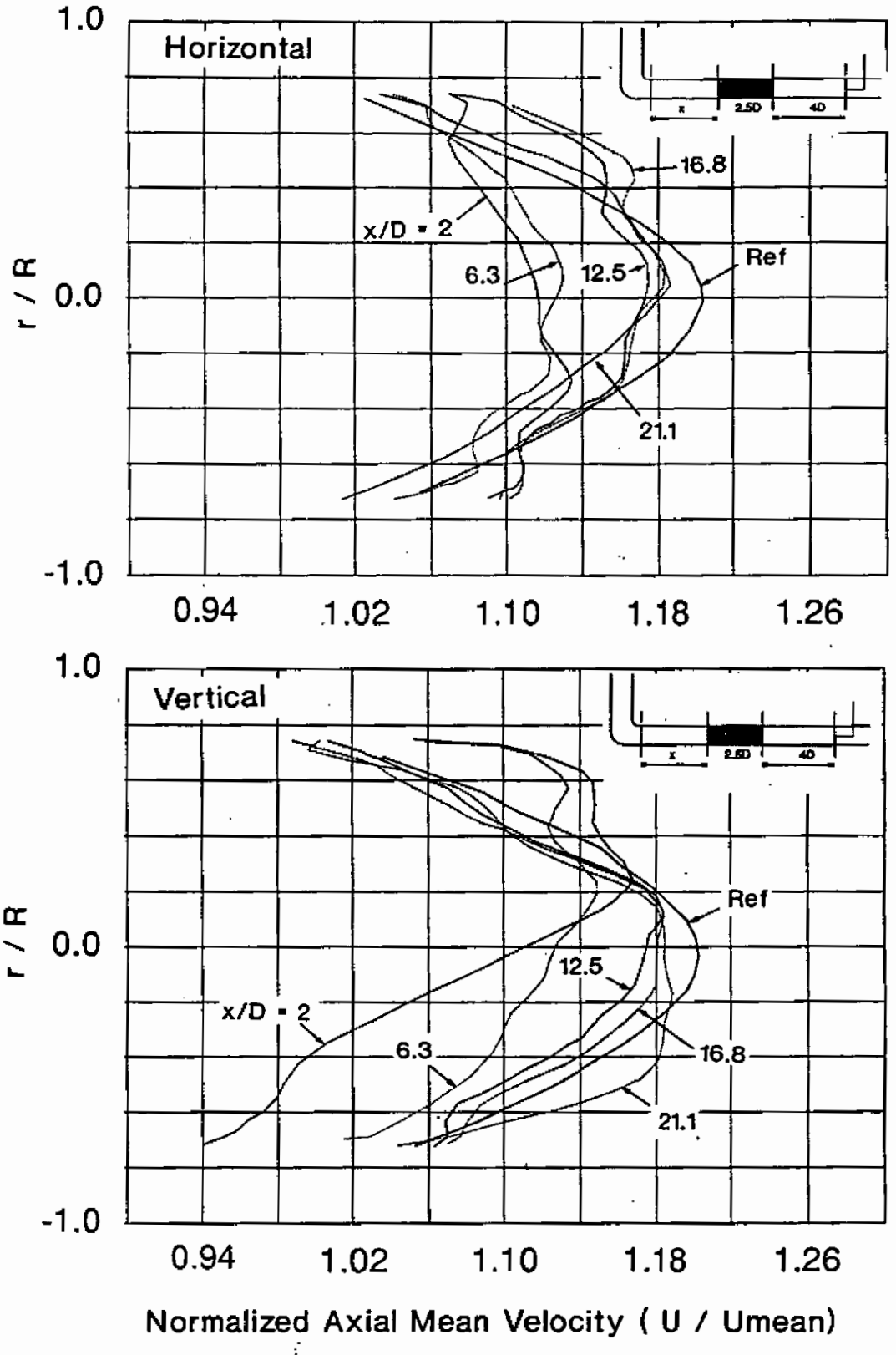

Fig. 5: **Axial Velocity Profiles in the Horizontal and Vertical Planes Downstream of Two Elbows In-Plane with a Tube Bundle at Different Locations and PST at 4 D Downstream of Tube Bundle Outlet ($Re = 8 \times 10^6$)**

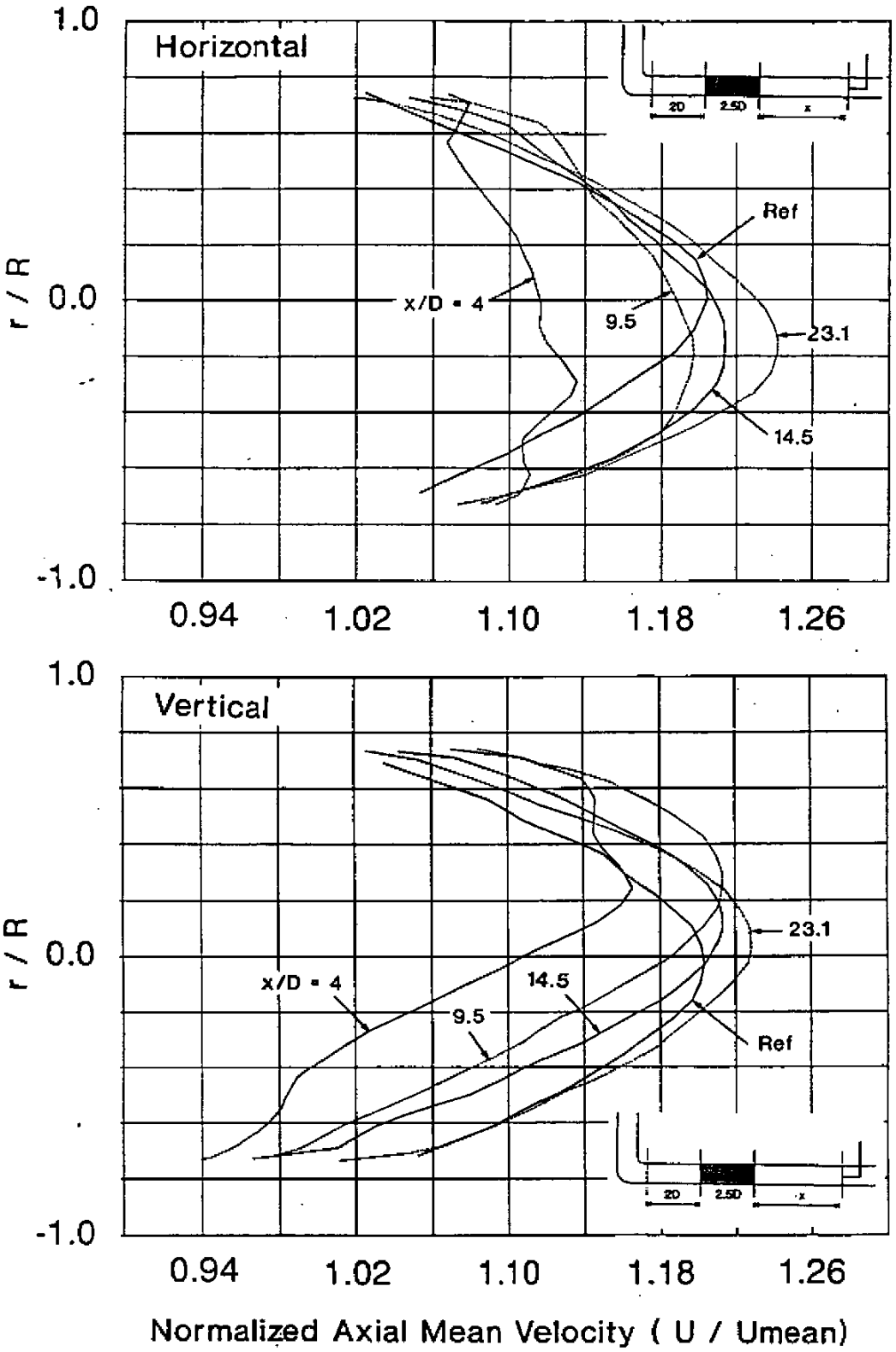

Fig. 6: **Axial Velocity Profiles in the Horizontal and Vertical Planes Downstream of Two Elbows In-plane with a Tube Bundle at Fixed Location (2 D from Elbow Outlet) and PST at Different Locations Downstream (Re = 8 x 10^6)**

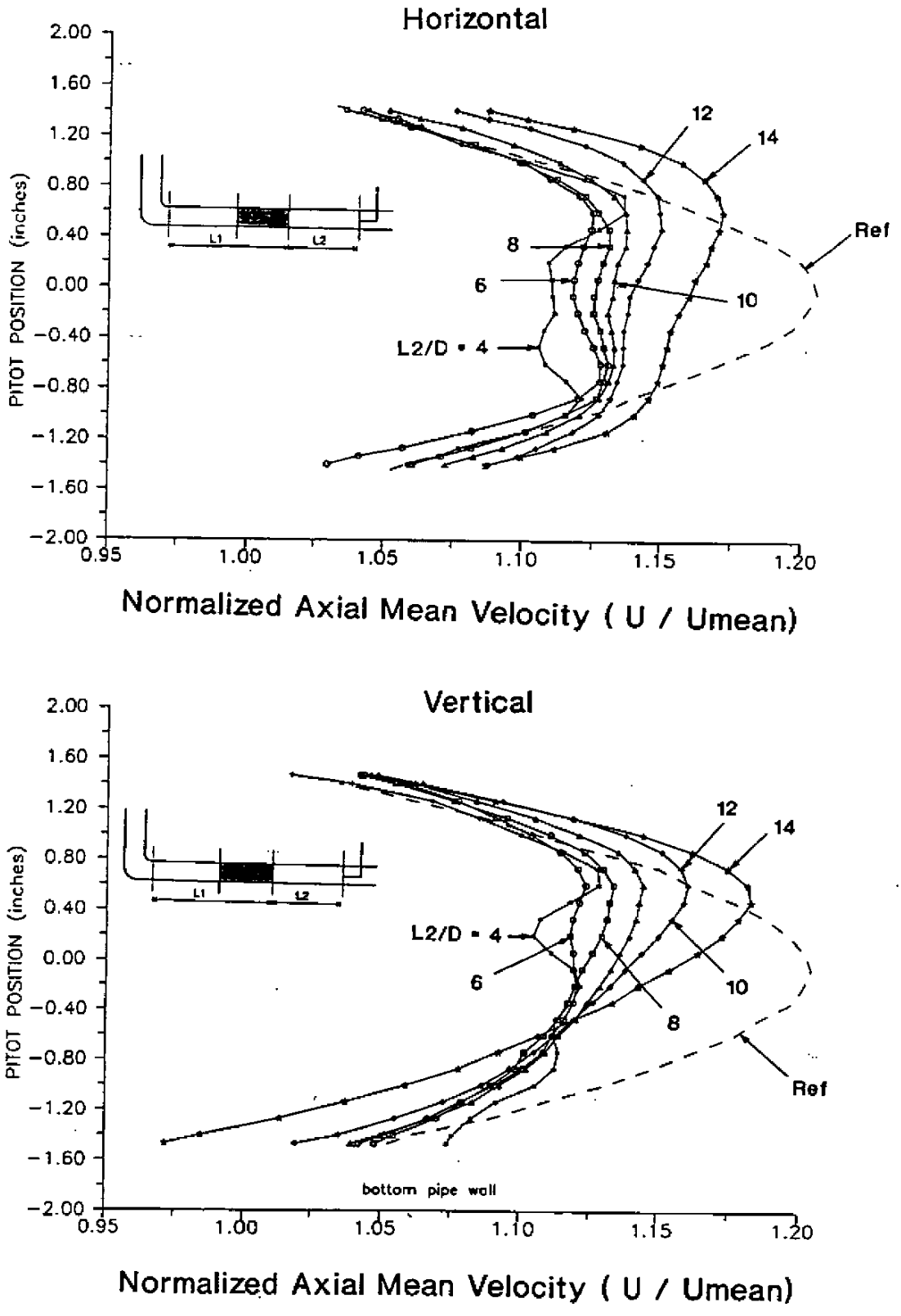

Fig. 7: **Axial Velocity Profiles in the Horizontal and Vertical Planes Downstream of Two Elbows In-plane with a Sliding Vane and PST at 19 D from Elbow Outlet ($Re = 8 \times 10^6$)**

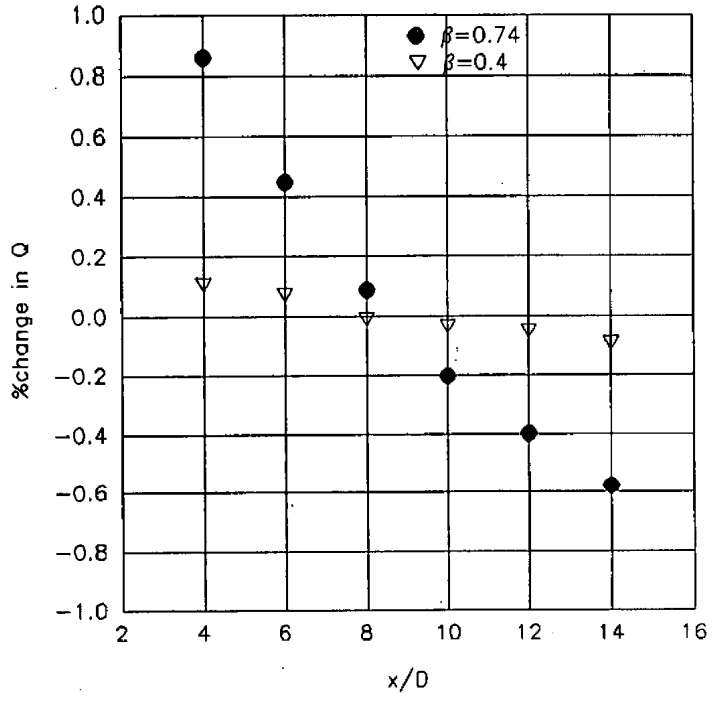

Fig. 8: Results of Comparitive Tests with a Sliding Vane and 19 D Meter Run for Two β-ratios of 0.4 and 0.74 ($Re = 8 \times 10^6$)

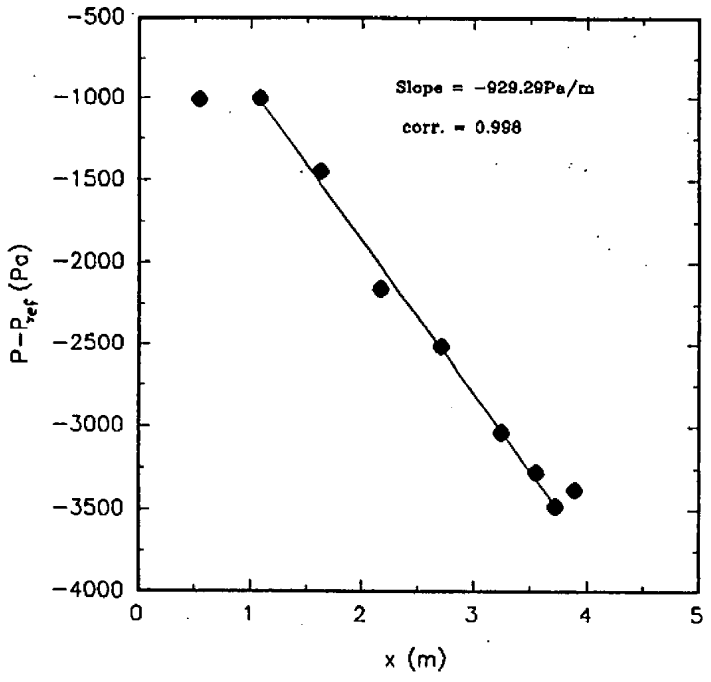

Fig. 9: Pressure Profile Along the 44 D Long Meter Run Upstream of the Reference Meter ($Re = 8 \times 10^6$)

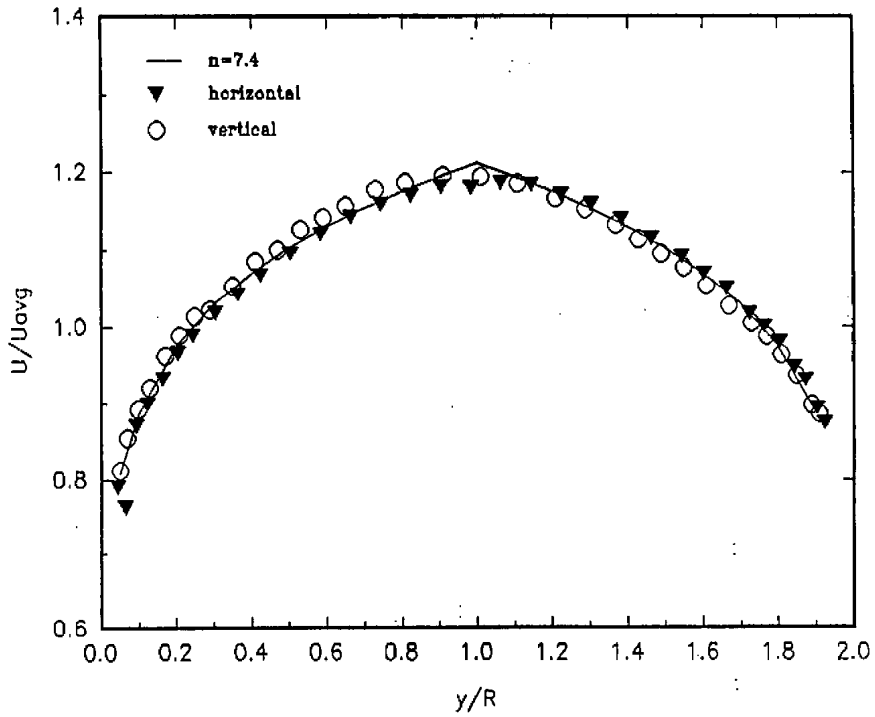

Fig. 10: Mean Axial Velocity Profiles in the Horizontal and Vertical Planes of a Fully Developed Flow on the Low Pressure Facility ($Re = 0.9 \times 10^5$)

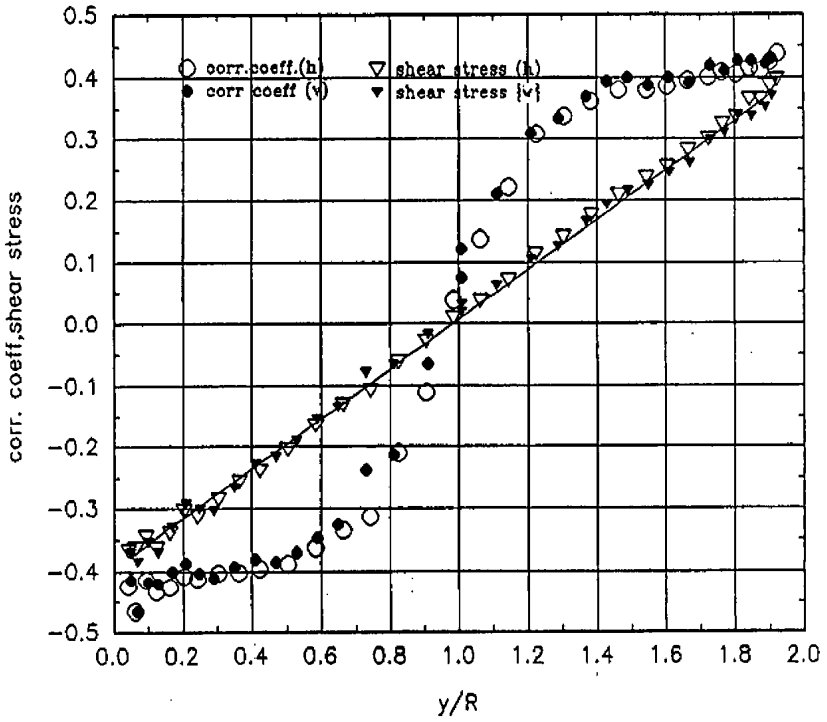

Fig. 11: Shear Stress and Correlation Coefficient for a Fully Developed Flow ($Re = 0.9 \times 10^5$)

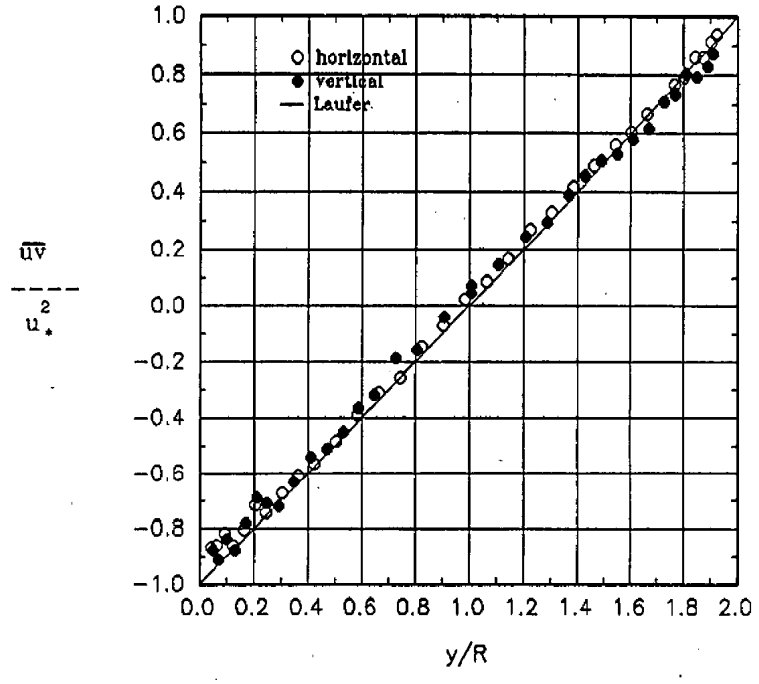

Fig. 12: Normalized Shear Stress with Frictional Velocity for a Fully developed Flow (Re = 0.9 x 10^5)

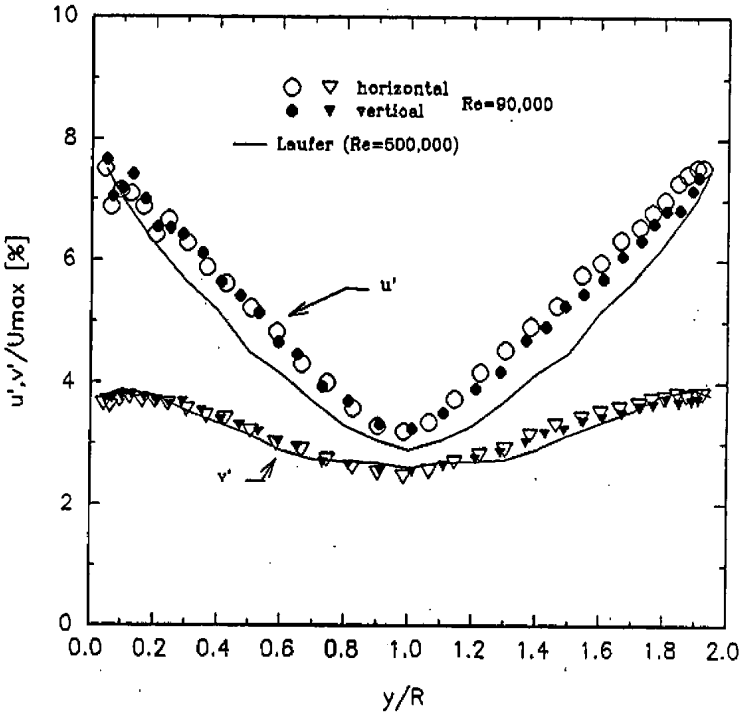

Fig. 13: Axial and Radial RMS Turbulent Intensities of a Fully Developed Flow (Re = 0.9 x 10^5)

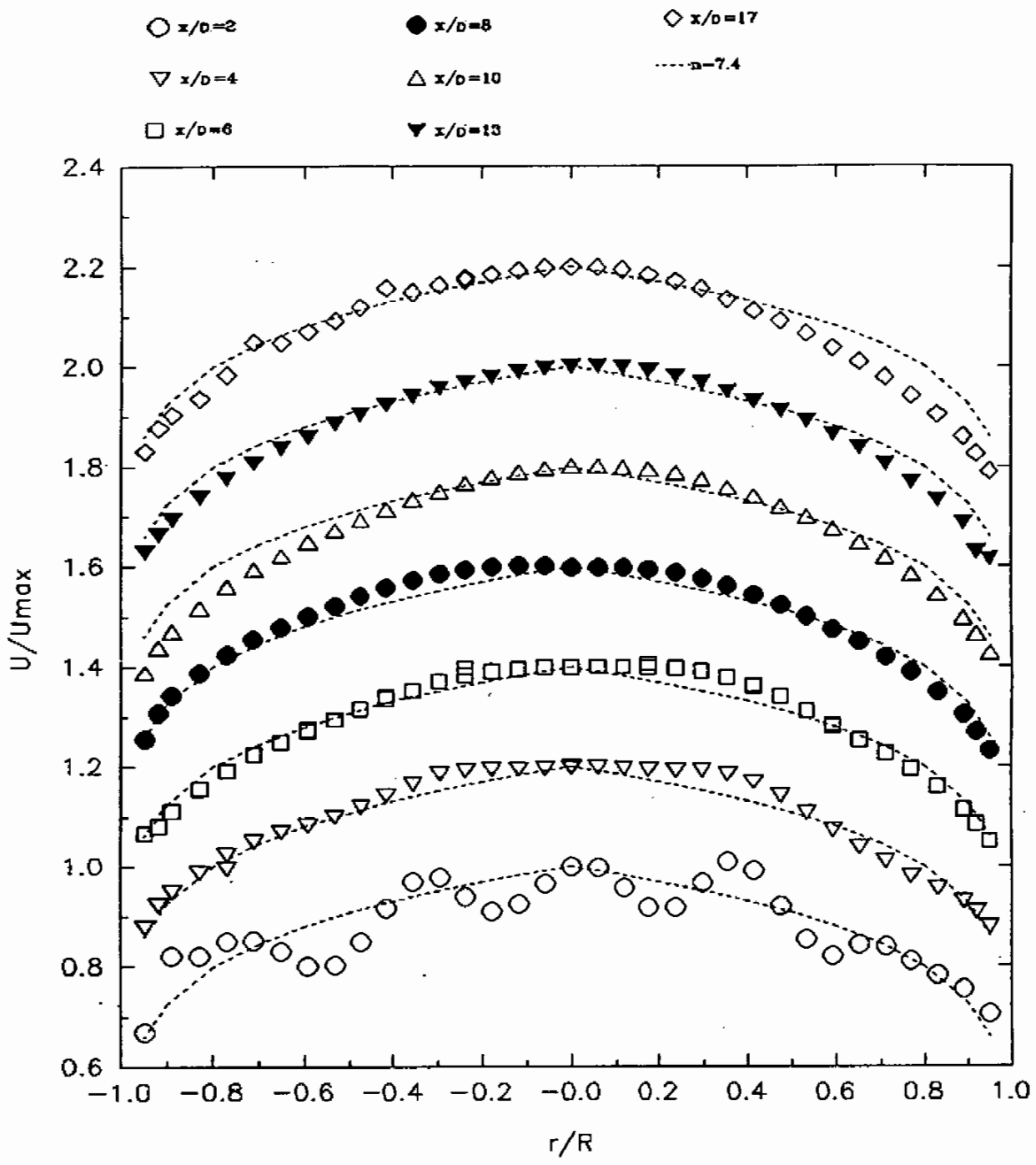

Fig. 14: Mean Axial Velocity Profiles Downstream of a Tube Bundle in Good Flow Conditions - ($Re = 0.9 \times 10^5$) (Note: Each Profile following x/D = 2 has been offset successivly by 0.2 units for separation of profile)

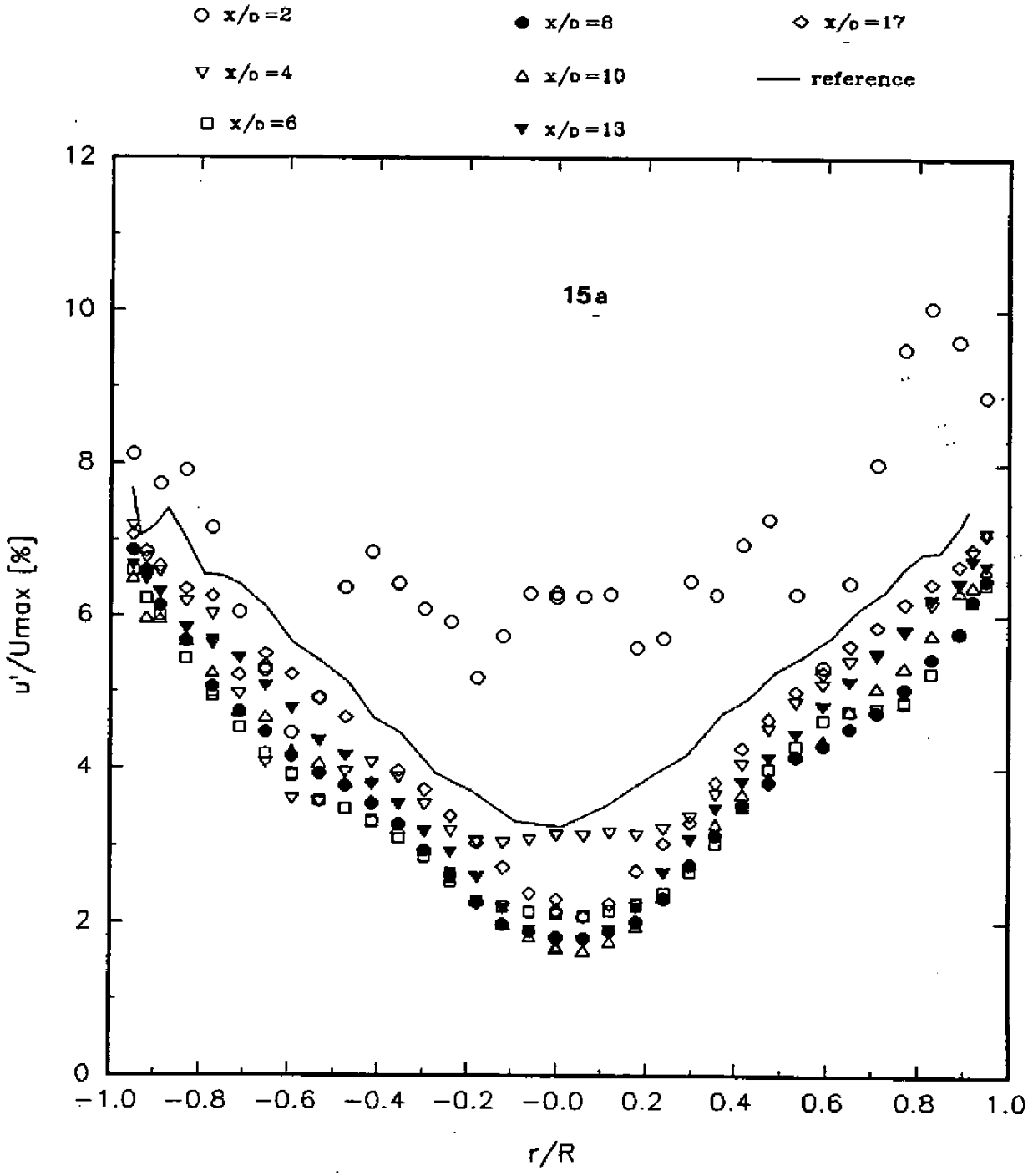
x/D=2
x/D=4
x/D=6
x/D=8
x/D=10
x/D=13
x/D=17
reference
15a
u'/Umax [%]
r/R
0
2
4
6
8
10
12
−1.0
−0.8
−0.6
−0.4
−0.2
−0.0
0.2
0.4
0.6
0.8
1.0

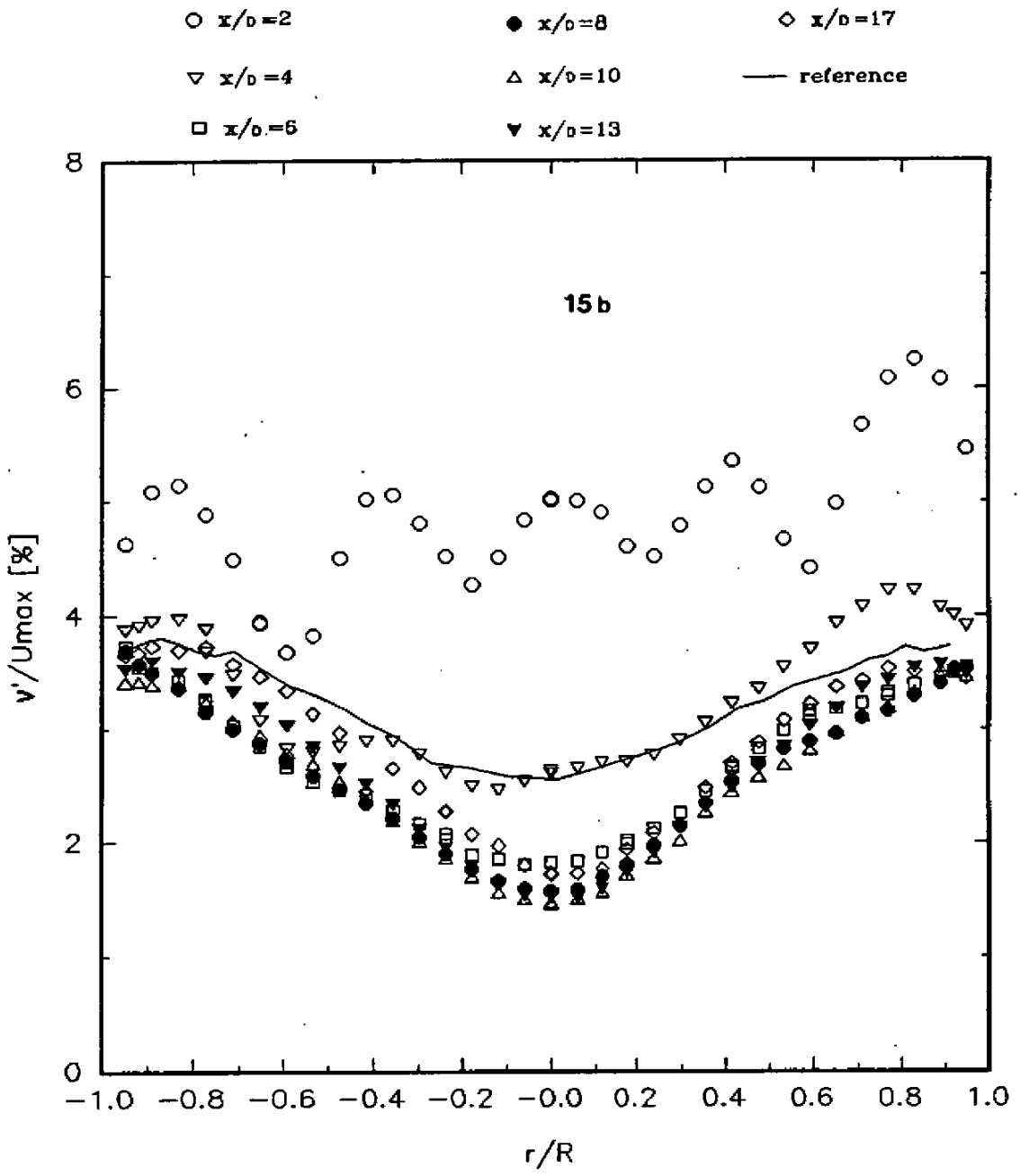

Fig. 15: Profiles of the Axial and Radial RMS Turbulent Velocities Normalized by U_{max}, Downstream of a Tube Bundle in Good Flow Conditions - ($Re = 0.9 \times 10^5$) (a - axial, b - radial)

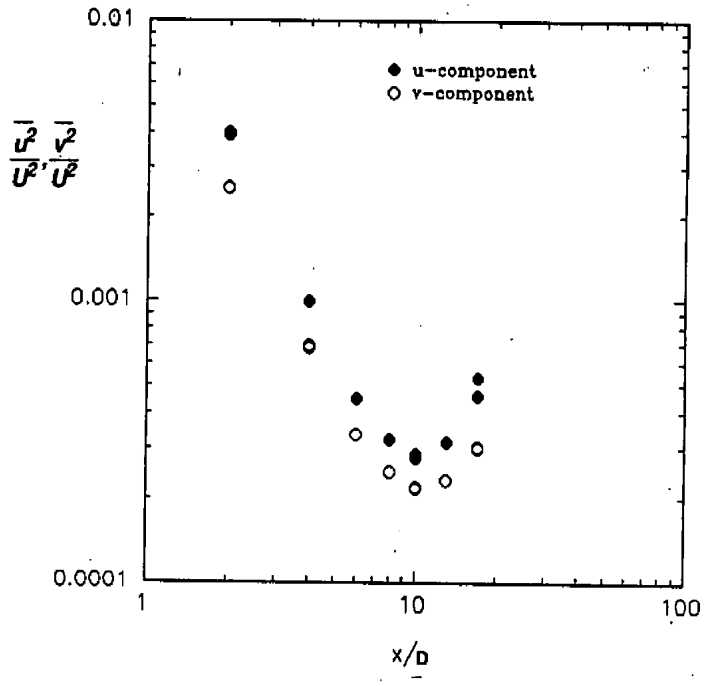

Fig. 16: Variation of the Normal Stresses on the Centerline Downstream of a Tube Bundle in Good Flow Conditions ($Re = 0.9 \times 10^5$)

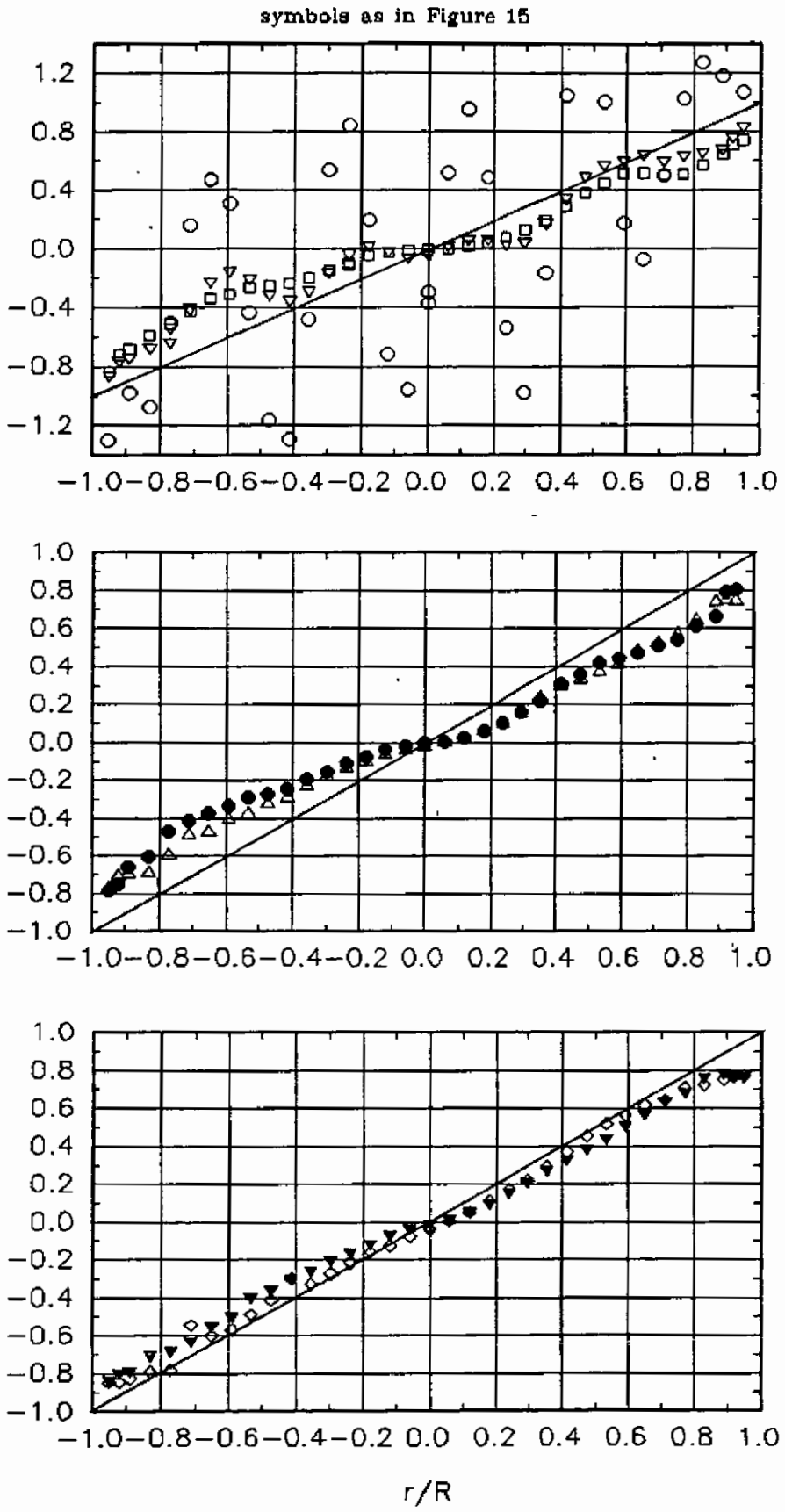

Fig. 17: Distribution of the Normalized Turbulent Shear Stress $\left(\overline{uv}/u_e^2\right)$ Downstream of a Tube Bundle in Good Flow Conditions (Re = 0.9 x 10^5)

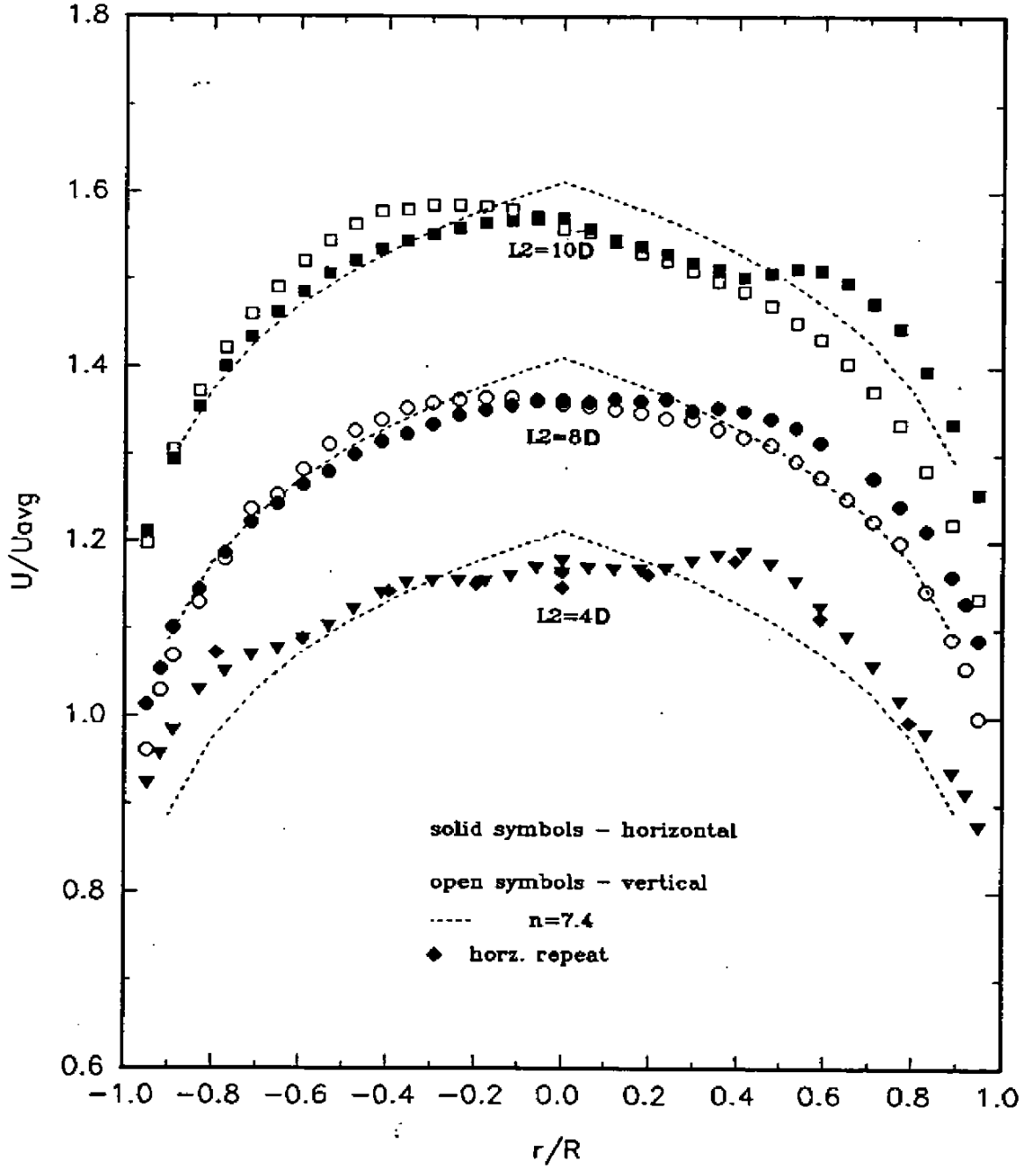

Note: Each data set following L2=4 has been offset by 0.2 units

Fig. 18: Mean Axial Velocity Profiles for Three Different Locations of a Tube Bundle Placed in 19 D Meter Run Downstream of a 90° Elbow - Re = 0.9 x 10^5

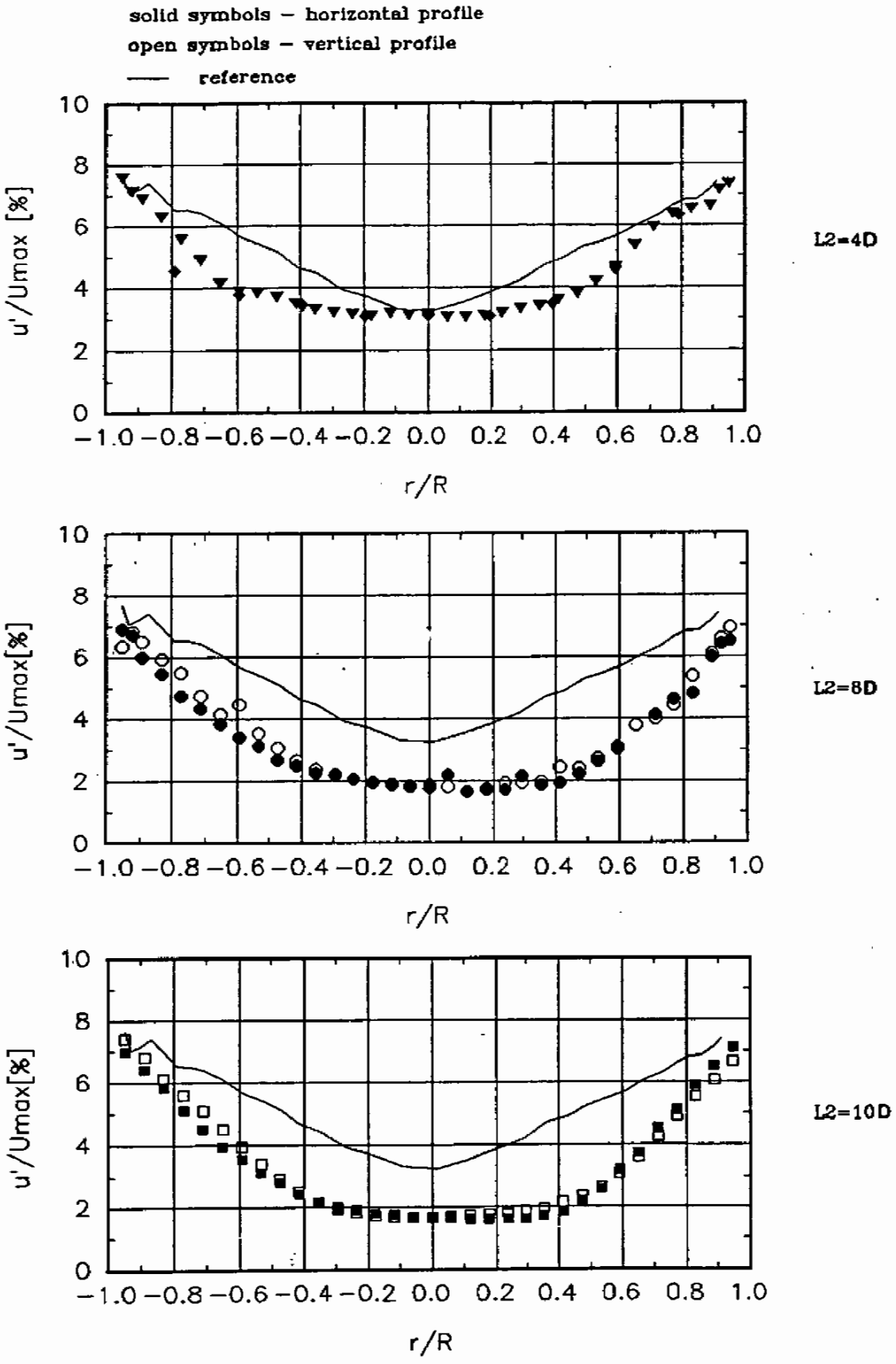

Fig. 19: Axial Turbulent Intensity (RMS) Downstream of a Tube Bundle Placed in 19 D Meter Run Downstream of a 90° Elbow (Re = 0.9 x 10^5)

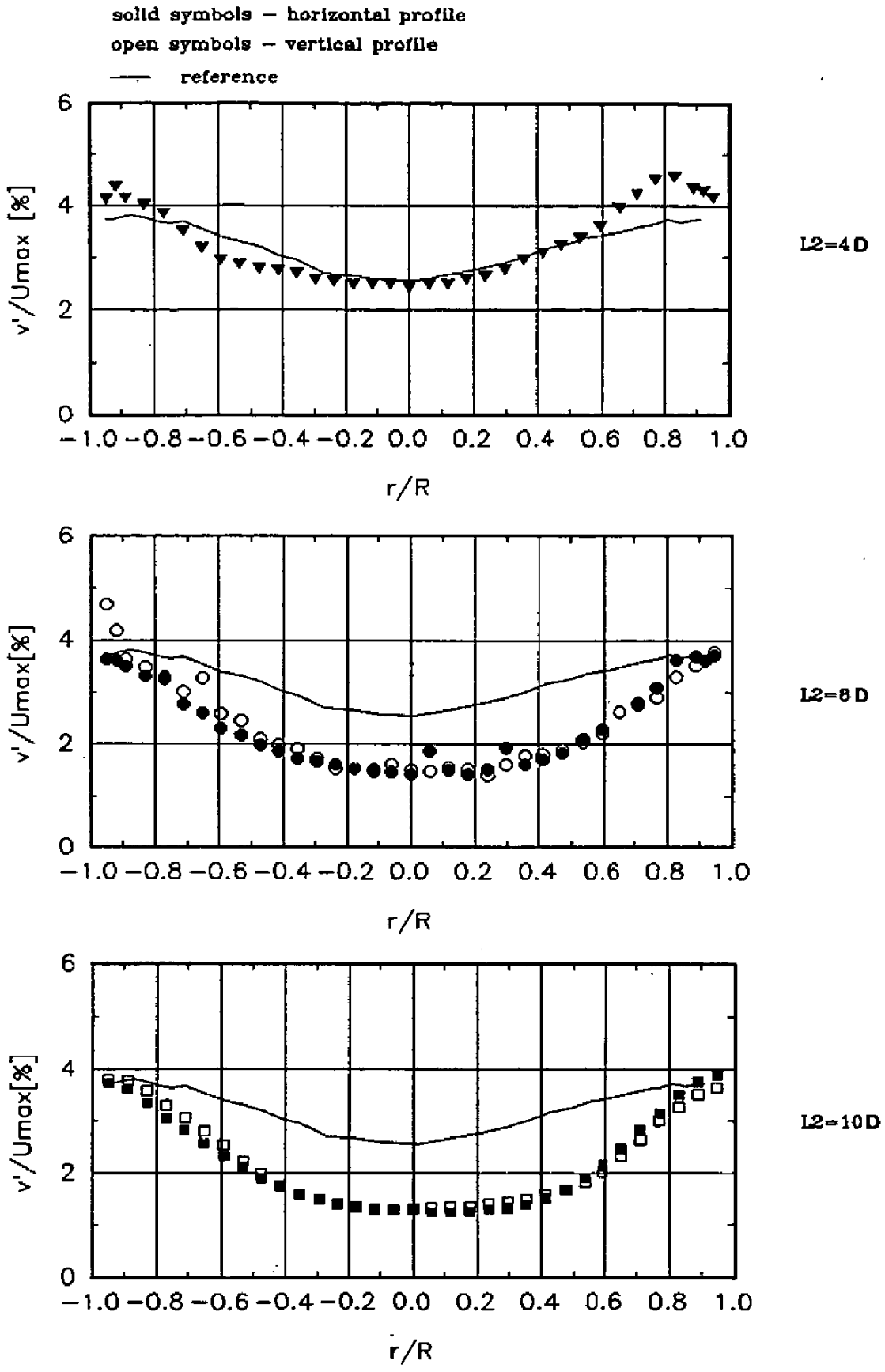

Fig. 20: Radial Turbulent Intensity (RMS) Downstream of a Tube Bundle Placed in 19 D Meter Run Downstream of a 90° Elbow (Re = 0.9 x 10^5)

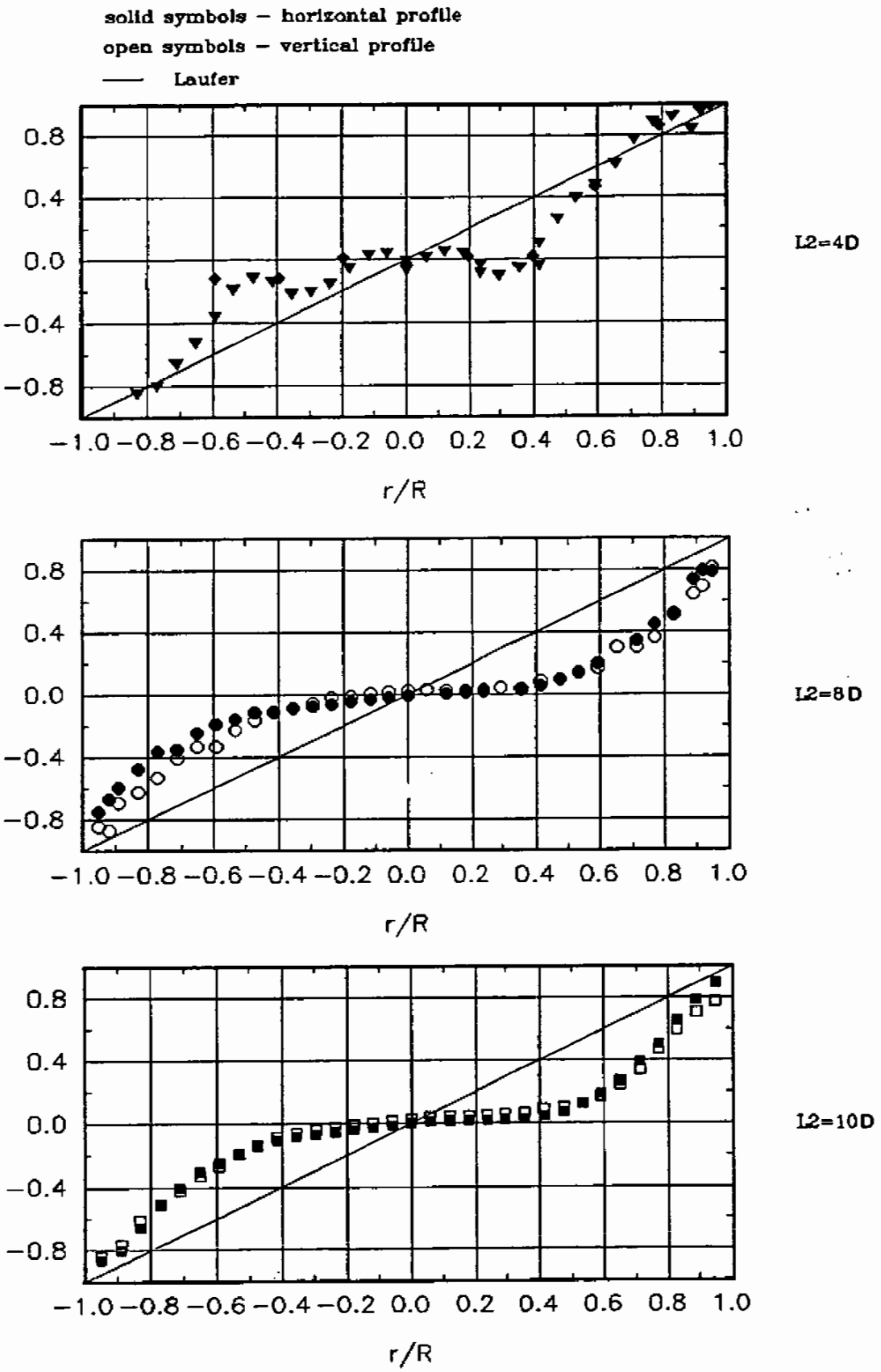

Fig. 21: Distribution of the Normalized Turbulent Shear Stress $\left(\overline{uv}/u_*^2\right)$ Downstream of a Tube Bundle in 19 D Meter Run Downstream of a 90° Elbow (Re = 0.9 x 10^5)

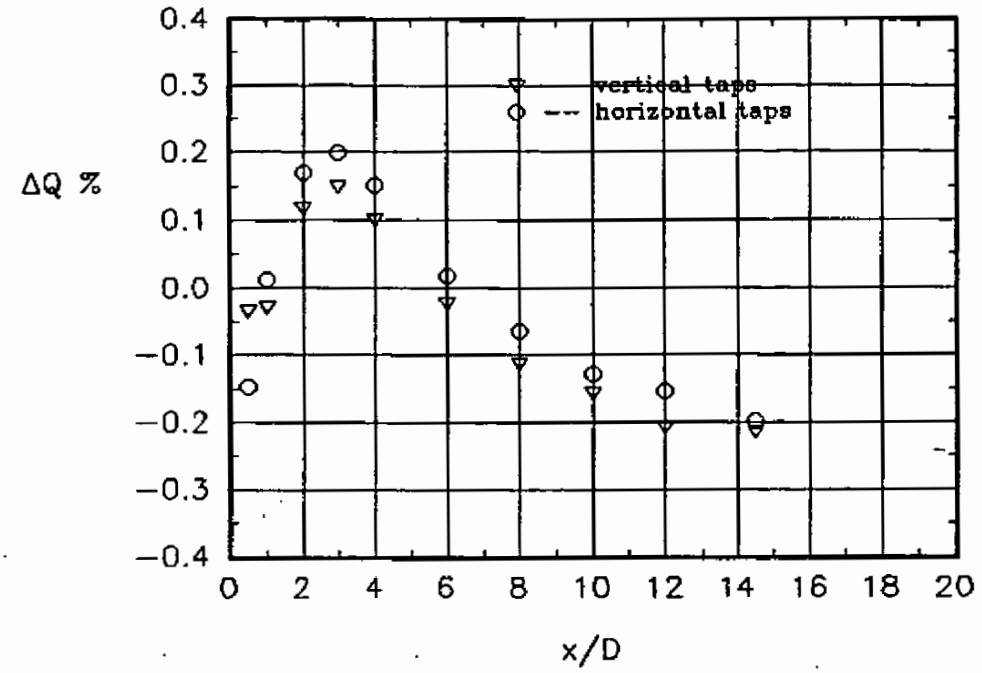

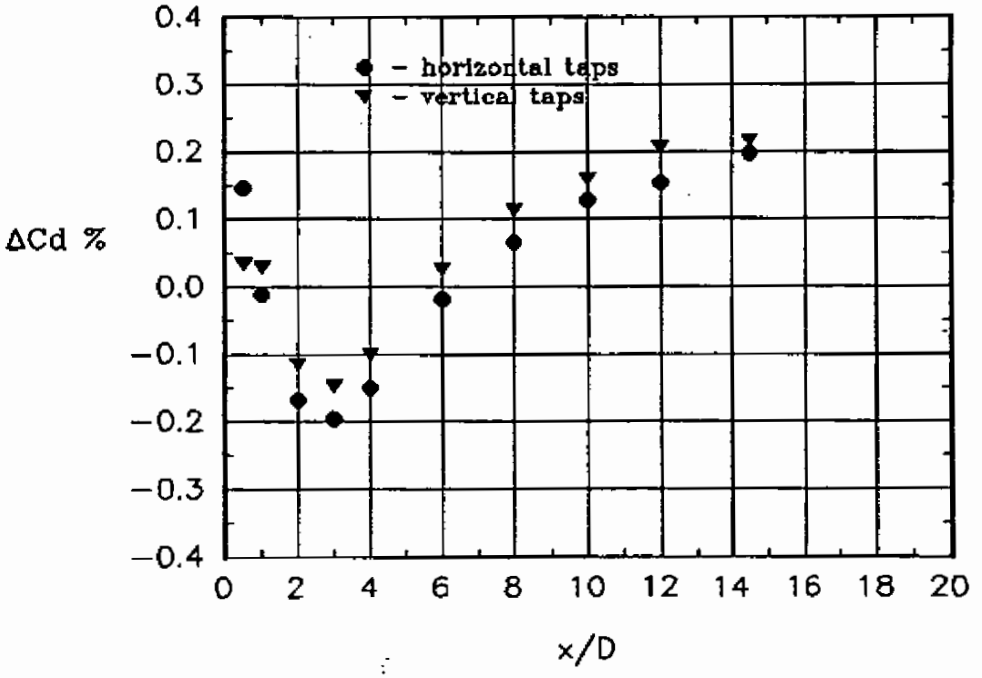

Fig. 22: Results of a Comparative Tests with a Pulling Vane in a 19 D Meter Run Downstream of a 90° Elbow ($Re = 1.4 \times 10^5$)